Int. J. Electrochem. Sci., 13 **(2018)** 2779 – 2790, doi: 10.20964/2018.03.26

International Journal of
ELECTROCHEMICAL
SCIENCE
www.electrochemsci.org

Short Communication

Electrochemical Corrosion and Mechanical Properties of Two Biomedical Titanium Alloys

Chien-Lung Huang, Tao-Hsing Chen [*], *Chia-Chin Chiang and Shih-You Lin*

Department of Mechanical Engineering, National Kaohsiung University of Applied Sciences, Kaohsiung 807, Taiwan
[*]E-mail: thchen@kuas.edu.tw

Received: 15 September 2017 / *Accepted:* 2 January 2018 / *Published:* 5 February 2018

The electrochemical corrosion and mechanical properties of two biomedical titanium alloys (Ti-13Nb-13Zr and Ti-15Mo) are investigated by means of electrochemical impedance spectroscopy (EIS) and a material testing system (MTS). The EIS results obtained in aerated Ringer's solution show that Ti-13Nb-13Zr has a higher corrosion resistance than Ti-15Mo. Consequently, of the two alloys, Ti-13Nb-13Zr has superior biocompatibility. Furthermore, the Quasi-static testing results reveal that Ti–13Nb-13Zr also has superior mechanical properties at strain rates in the range of 10^{-3}~$10^{-1}s^{-1}$.

Keywords: electrochemical, corrosion, Ti-13Nb-13Zr alloy, Ti-15Mo alloy, mechanical properties, strain rate.

1. INTRODUCTION

Titanium (Ti) and its alloys have excellent corrosion resistance, a light weight, and a good mechanical performance. As a result, they are widely used in many sports, medical, aerospace, marine and chemical applications [1-5]. Among the various Ti alloys available, Ti-6Al-4V is one of the most commonly used. However, it is associated with various health issues due to the gradual release of toxic Al and V elements over time [6-8]. As a result, it has only limited potential for biomedical use. To address this problem, various Ti alloys composed of non-toxic and non-allergic elements such as Mo, Nb, Zr, Ta and Sn have been proposed in recent years [9-16].

Of these elements, Nb, Zr and Mo are regarded as particularly suitable β-phase stabilizers for Ti alloy. Moreover, Ti-13Nb–13Zr and Ti–15Mo have a low elastic modulus and a high tensile strength, and are thus ideally suited for surgical implant applications. However, the success of

biomedical implants depends not only on the mechanical properties of the implant material (e.g., a low elastic modulus and good formability), but also the anti-corrosion properties.

The literature contains many investigations into the microstructure, fatigue properties, phase transformation and as-cast properties of Ti alloys [17–20]. However, little information is available regarding the corrosion behaviour and mechanical properties of Ti-13Nb-13Zr and Ti–15Mo. Therefore, the present study uses an electrochemical impedance spectroscopy (EIS) technique to examine the corrosion resistance of Ti-13Nb-13Zr and Ti-15Mo alloys in simulated body fluid (SBF). In addition, a Materials Testing System (MTS) is used to examine the mechanical properties of the two alloys under strain rates ranging from 10^{-3}~10^{-1} s^{-1}. The compositions and microstructures of the various specimens are examined via energy-dispersive X-ray spectroscopy (EDS) and transmission electron microscopy (TEM), respectively.

2. MATERIAL PREPARATION AND EXPERIMENTAL PROCEDURE

Ti-13Nb-13Zr and Ti-15Mo were purchased from President Titanium Inc., USA, in the form of bars with a diameter of 12 mm. Prior to delivery, the Ti-13Nb-13Zr alloy was solution-treated at 1000 ºC under an Ar atmosphere for 24 h, quenched in water, aged at 500 ºC for 4 h, and then finally cooled in air. Meanwhile, the Ti-15Mo alloy was solution-treated in a vacuum for 5 h at a temperature higher than the β-transus temperature of the alloy (i.e., 850℃[21]) and then quenched in ice water.

The electrochemical corrosion properties of the two alloys were investigated in an aerated Ringer's solution composed of 9.0 gL^{-1} NaCl, 0.43 gL^{-1} KCl, 0.24 gL^{-1} $CaCl_2$ and 0.20 gL^{-1} $NaHCO_3$. (See my comment at the end of the paragraph.) The EIS measurements were obtained using a Compactstat 1030 Ivium potentiostat with a three-electrode corrosion cell consisting of a working electrode (Ti-13Nb-13Zr or Ti-15Mo) with a surface area of 1 cm^2, a platinum (Pt) wire counter-electrode, and an Ag/AgCl reference electrode (saturated in KCl solution).

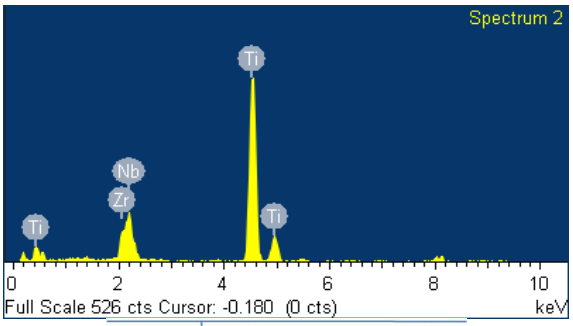

Element	Weight%	Atomic%
Ti K	73.8	79.57
Zr L	12.63	9.79
Nb L	13.52	10.64
Totals	100.00	

(a)

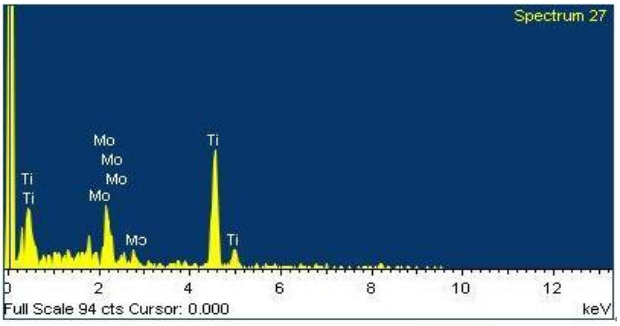

Element	Weight%	Atomic%
Ti K	84.71	90.2
Mo L	15.29	9.8
Totals	100.00	

(b)

Figure 1. EDS chemical composition results for (a) Ti-13Nb-13Zr; (b) Ti-15Mo.

The chemical compositions of the as-received samples were examined via EDS analysis. The results presented in Figs. 1(a) and 1(b) confirm that the chemical compositions of the two alloys are closely related to their nominal compositions. The microstructures of the alloy specimens were observed using a JEOL-3010 transmission electron microscope operating at 300 kV. Thin foils were prepared for TEM observation by twin-jet electropolishing with an agitation voltage of 35 V in a solution consisting of 60 mL $HClO_4$, 590 mL methanol and 350 mL ether-monobutylethylene at a temperature of -20 ºC.

The mechanical properties of the two alloys were investigated under room temperature conditions (25ºC) at strain rates of 10^{-3} s^{-1}, 10^{-2} s^{-1} and 10^{-1} s^{-1} using an MTS 810 Materials Testing System. The quasi-static tests were performed using cylindrical specimens machined from the as-received bars with a length of 7±0.1 mm and a diameter of 7.2 mm and then finished to a final diameter of 7±0.1 mm via a centre-grinding process.

3. RESULTS AND DISCUSSION

3.1. Electrochemical corrosion properties

In general, biomedical Ti alloys have good corrosion resistance due to the natural formation of a thin but dense oxide film (TiO_2) on the surface. The formation and stability of the passive film is usually evaluated by means of anodic polarization tests. The Tafel extrapolation was introduced to describe the application of mixed potential theory to aqueous corrosion.

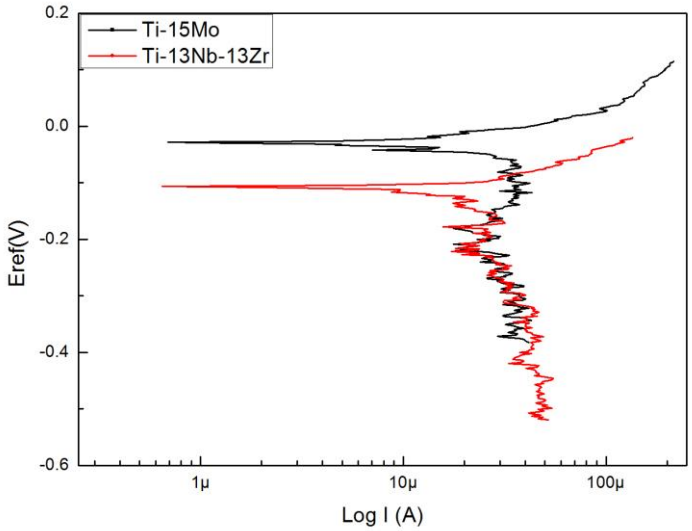

Figure 2. Polarization curves of Ti-13Nb-13Zr and Ti-15Mo in aerated Ringer's solution at 25℃ (scan rate: 0.050 V/min).

Figure 2 shows the polarization curves obtained for the current Ti-13Nb-13Zr and Ti-15Mo alloys. It is seen that the two curves are qualitatively similar and are characteristic of passive film formation. However, the corrosion potential of the Ti-13Nb-13Zr alloy (-0.11 V) is significantly lower than that of the Ti-15Mo alloy (-0.029 V). Furthermore, as shown in Table 1, the corrosion density of Ti-13Nb-13Zr (2.06 μA/cm^2) is also lower than that of Ti-15Mo (3.66 μA/cm^2). The reason for the Ti-13Nb-13Zr alloy has higher corrosion properties is that the passive film consists mainly of TiO_2 with a trace quantity of Nb_2O_5 and ZrO_2. The combination of passive film TiO2 layer with Nb_2O_5 or ZrO_2 will enhance the structural integrity of the oxide film [22-24]. Some literatures [24] report the Ti-6Al-4V alloy has well corrosion resistance than Ti-13Nb-13Zr alloy. But the Ti-13Nb-13Zr alloy has well wear resistance and non-toxic property than Ti-6Al-4V alloy, and Ti-13Nb-13Zr alloy can replace the Ti-6Al-4V alloy to utilize in the biomaterials implant.

Table 1. Corrosion potential and corrosion current density of Ti-13Nb-13Zr and Ti-15Mo in Ringer's solution.

Alloy\parameter	Ti-13Nb-13Zr	Ti-15Mo
$E_{corr.}$ (V)	-0.11	-0.029
$i_{corr.}$ (μA/cm^2)	2.06	3.66

In other words, of the two alloys, Ti-13Nb-13Zr has a superior anticorrosion performance. The improved corrosion resistance can be attributed to the presence of Nb, which prompts an annihilation of the anion vacancies in the crystal lattice of the TiO_2 surface layer.

3.2. Mechanical properties

Figures 3(a) and 3(b) show the true stress-strain curves of the Ti-13Nb-13Zr and Ti-15Mo specimens deformed at 25 ºC under quasi-static strain rates of 10^{-3} s^{-1}, 10^{-2} s^{-1} and 10^{-1} s^{-1}. It is seen that for both alloys, the flow stress increases with increasing strain and strain rate. Furthermore, comparing the two figures, it is observed that for a given strain rate, the Ti-13Nb-13Zr specimen has a higher flow stress than the Ti-15Mo specimen. In other words, the Ti-13Nb-13Zr alloy has a greater work hardening ability than the Ti-15Mo alloy. This suggests that the element of Nb can enhance the mechanical property; due to the Nb have higher stability of β phase. Therefore, it results in a longer time for energy accumulation within the deformed microstructure and hence a greater mobility at the boundaries for grain growth and dislocation annihilation. It can be identified in the microstructure evolution.

Table 2. Mechanical properties of Ti-13Nb-13Zr and Ti-15Mo deformed at 25ºC under strain rates of 10^{-3}~10^{-1} s^{-1}.

	Strain Rate (s^{-1})	Yielding Strength, A (MPa)	Strength coefficient, B (MPa)	Work hardening coefficient, n
Ti-13Nb-13Zr	0.001	527.3	944.4	0.422
	0.01	539.3	955.5	0.424
	0.1	551.4	976.1	0.427
Ti-15Mo	0.001	434.7	451	0.286
	0.01	443.2	451.6	0.291
	0.1	447.2	452.3	0.296

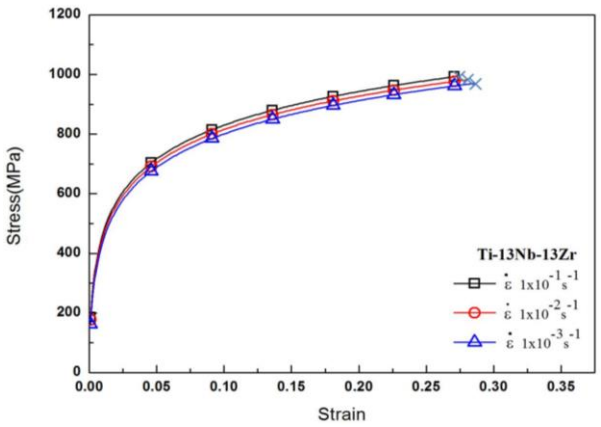

(a)

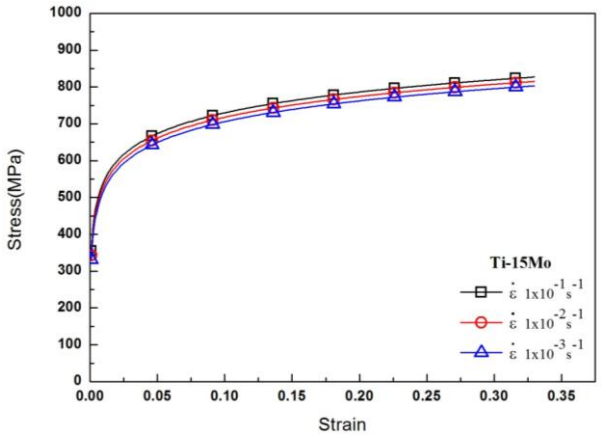

(b)

Figure 3. Flow stress-strain curves of (a) Ti-13Nb-13Zr alloy; (b) Ti-15Mo alloy deformed at strain rates of 10^{-1} s^{-1}~10^{-3} s^{-1}.

The work hardening behaviour of the two alloys can be evaluated using the empirical relation $\sigma = A + B\varepsilon^n$, where A is the yielding strength, B is the strength coefficient, and n is the work hardening coefficient. Table 2 shows the values of A, B and n obtained for the Ti-13Nb-13Zr and Ti-15Mo specimens, respectively, by fitting the stress-strain data presented in Figs. 3(a) and 3(b) using this empirical relation. It is seen that the yielding strength, strength coefficient and work hardening coefficient all increase with increasing strain rate for both alloys. However, it is also seen that, for a given strain rate, the yielding strength, strength coefficient and work hardening coefficient of Ti-13Nb-13Zr are higher than those of Ti-15Mo.

3.3. Strain rate effect

The flow stress property of engineering materials under different strain rates conditions has attracted experimental and theoretical interest [25-29]. The results have shown that the flow stress increases with increasing strain rate. The different deformation mechanisms have been proposed to account for the microstructural changes observed following deformation under different strain rate conditions. In this section, we investigate firstly the effect of the strain rate on the mechanical properties of the two alloys. The strain rate effect can be quantified using the following strain rate sensitivity parameter [30, 31]:

$$\beta = \partial\sigma / \partial\dot{\varepsilon} = \left(\sigma_2 - \sigma_1\right) / \ln\left(\dot{\varepsilon}_2 / \dot{\varepsilon}_1\right),$$

where the flow stresses σ_2 and σ_1 are obtained from tests conducted at quasi-static strain rates of $\dot{\varepsilon}_2$ and $\dot{\varepsilon}_1$, respectively.

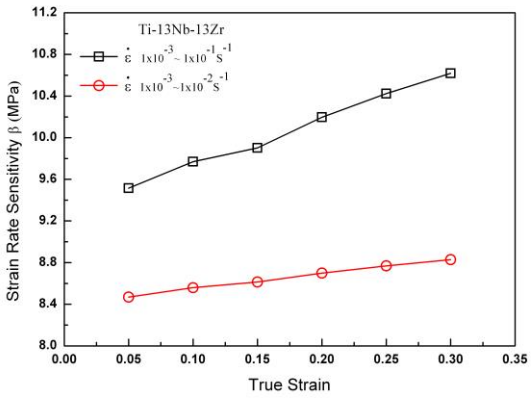

(a)

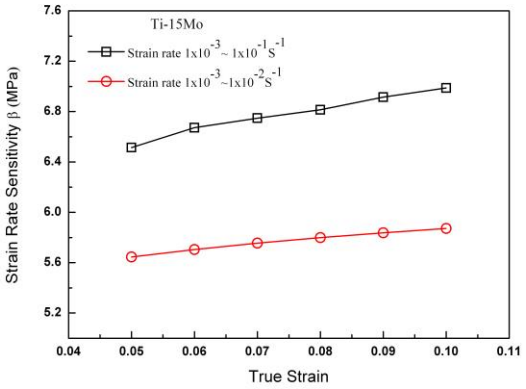

(b)

Figure 4. Variation of strain rate sensitivity with true strain for (a) Ti-13Nb-13Zr alloy; (b) Ti-15Mo alloy.

Figure 4(a) shows the variation of the strain rate sensitivity with the strain for the Ti-13Nb-13Zr alloy under strain rate ranges of $10^{-3} \sim 10^{-1}$ s^{-1} and $10^{-3} \sim 10^{-2}$ s^{-1}, respectively. It is observed that for a given strain, the strain rate sensitivity increases with increasing strain rate. A similar tendency is noted for the Ti-15Mo alloy in Fig. 4(b). However, comparing the two figures, it is found that Ti-13Nb-13Zr has a greater strain rate sensitivity.

Table 3. Comparison of the corrosion property with other alloys

Tafel Parameters	E_{corr} (V)	I_{corr} (μA/cm^2)
Ti-13Nb-13Zr [this study]	-0.11	2.06
Ti-15Mo [this study]	-0.029	3.66
γTiAl alloy[32]	-0.428	1.94
Ti-6Al-4V [33]	-0.430	1.9
316L[34]	-0.202	12.97

Table 4. Comparison of the mechanical property with other alloys

Alloy / property	Ti-13Nb-13Zr	Ti-15Mo	Ti-6Al-4V [35]	Ti-6Al-7Nb [36]
Flow Strength, (Strain rate of 10^{-3})	950 MPa	750 MPa	945 MPa	776 MPa

Table 3 and Table 4 are the comparison of mechanical and electrochemical properties with other alloys. From these tables, they can be seen that the Ti-13Nb-13Al alloy in this study has well properties on mechanical and corrosion properties than other alloys. Although, the Ti-6Al-4V alloy has high corrosion property than Ti-13Nb-13Al alloy, but the Ti-13Nb-13Al alloy owns more biomedical safety than Ti-6Al-4V alloy.

3.4. Microstructural observations

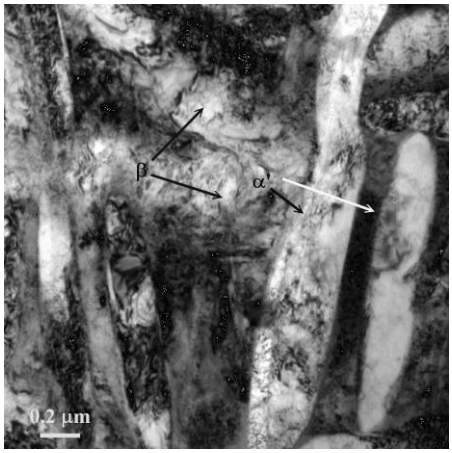

(a)

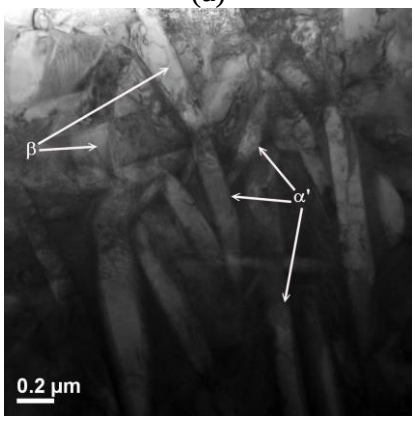

(b)

Figure 5. TEM images showing α' and β phases in as-received (a) Ti-13Nb-13Zr alloy; (b)Ti-15Mo alloy.

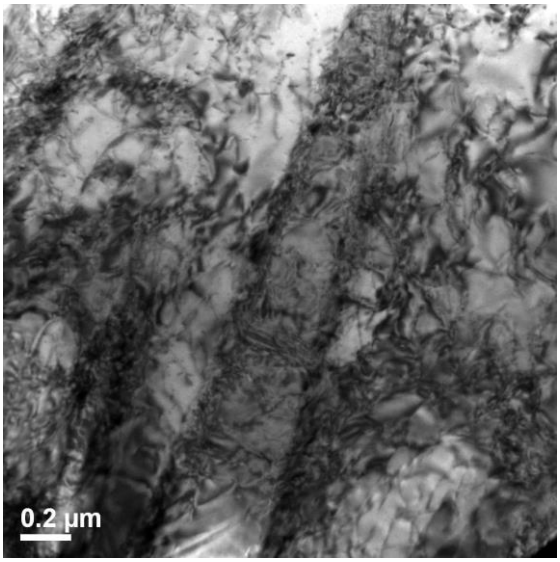

(a)

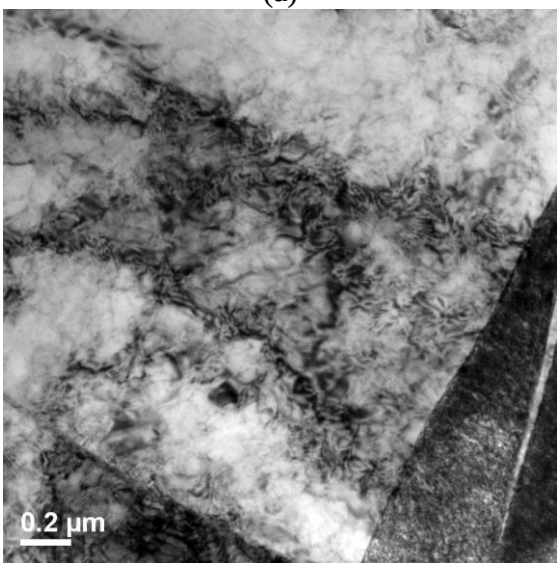

(b)

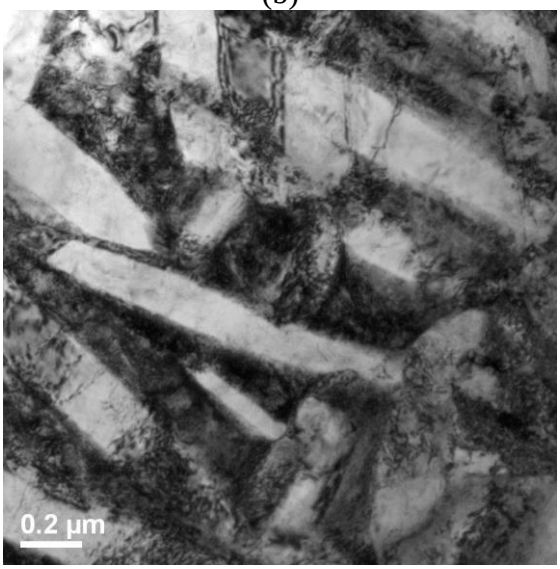

(c)

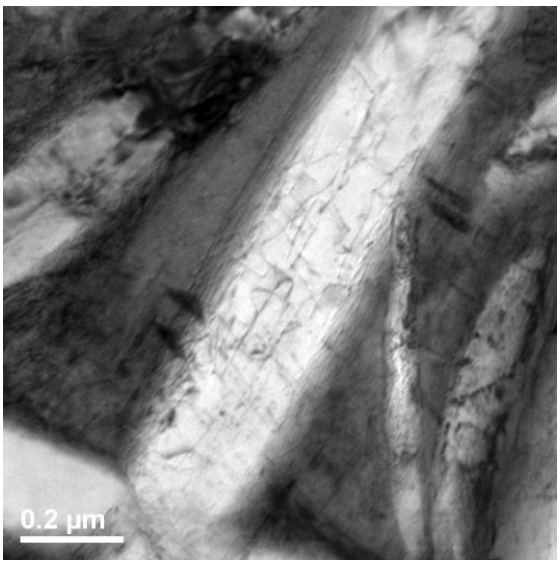

(d)

Figure 6. TEM micrographs of Ti-13Nb-13Zr alloy deformed at strain rates of (a) 10^{-1} s^{-1}; (b) 10^{-3} s^{-1}; Ti-15Mo alloy deformed at strain rates of (c) 10^{-1} s^{-1}; (d) 10^{-3} s^{-1}.

Figures 5(a) and 5(b) present TEM bright-field images of the as-received Ti-13Nb-13Zr and Ti-15Mo alloys, respectively.

The microstructures of both alloys contain alpha prime martensite (α') phase and sub-microscopic β phase. The Ti-13Nb-13Zr alloy contains slightly less α' phase than the Ti-15Mo alloy. However, it contains a greater amount of Nb-rich β phase, and therefore has a superior anticorrosion resistance (as shown in Fig. 2). Figures 6(a) and 6(b) present TEM images of the Ti-13Nb-13Zr specimens deformed at strain rates of 10^{-1} s^{-1} and 10^{-3} s^{-1}, respectively. Observing the two figures, it is found that the dislocation density and volume fraction of β phase increase with increasing strain rate. The higher β volume fraction and dislocation multiplication rate result in a strengthening effect (as evidenced by the flow stress-strain curves presented in Fig. 3(a)). A similar response is observed for the Ti-15Mo alloy specimens deformed at strain rates of 10^{-1} s^{-1} and 10^{-3} s^{-1}, respectively (see Figs. 6(c) and 6(d).

However, comparing Figs. 6(a) and 6(c) (and Figs. 6(b) and 6(d)), it is seen that the Ti-13Nb-13Zr alloy has a higher dislocation density and β phase than the Ti-15Mo alloy. As a result, for a given strain and strain rate, the flow stress in the Ti-13Nb-13Zr alloy is higher than that in the Ti-15Mo alloy. Overall, the microstructural observations presented in Fig. 6 suggests that the flow behaviour of the present Ti-13Nb-13Zr and Ti-15Mo alloy specimens is directly related to different duplex structures of β phase and the density of the dislocations [37, 38].

4. CONCLUSION

The electrochemical corrosion and mechanical properties of two biomedical alloys (Ti-13Nb-13Zr and Ti-15Mo) have been investigated and compared. It has been shown that Ti-13Nb-13Zr has

both a better anticorrosion performance in SBF than Ti-15Mo and superior mechanical properties. TEM observations have suggested that the superior performance of Ti-13Nb-13Zr is the result of a lower volume fraction of α' phase, a greater volume fraction of Nb-rich β phase, and a higher dislocation density.

ACKNOWLEDGEMENTS
The authors gratefully acknowledge the financial support provided to this study by the Ministry of Science and Technology of the Republic of China under Grant No. MOST 102-2221-E-151-006-MY3.

References

1. M. Long and H. J. Rack, *Biomaterials*, 19 (1998) 1621-1639.
2. Niinomi M. Recent metallic materials for biomedical applications, *Metall. Mater. .Trans. A.* 33 (2002) 477.
3. S.B. Gabriel, C.A. Nunes and G.A. Soares, *Artif. Organs.*, 32 (2008) 299.
4. W.F. Ho, C.P. Ju and J.H. Chern Lin, *Biomaterials*, 20 (1999) 2115.
5. P.L. Ferrandini, F.F. Cardoso, S.A. Souza, C.R. Afonso and R. Caram, *J. Alloys Comp*., 433 (2007) 207.
6. K. Wang, *Mat. Sci. Eng. A*, 213 (1996) 134
7. P.R. Walker, J. LeBlanc, M. Sikorska, *Biochemistry*, 28 (1989) 3911.
8. Y. Okazaki, S. Rao, Y. Ito and T. Tateishi, *Biomaterials*, 19 (1998) 1197.
9. S.G. Fedotov, T.V. Chelidez, Y.K. Kovneristy and V.V. Sanadze, *Phys. Met. Metall.*, 62 (1986) 109.
10. K. H. Park, M.J. Hwang, H.J Song and Y. J. Park, *Int. J. Electrochem. Sci.*, 11 (2016) 5552.
11. C. Vasilescu, P. Drob, E. Vasilescu, P. Osiceanu, S. I. Drob and M. V. Popa, *Int. J. Electrochem. Sci.*, 8 (2013) 10733.
12. B.S.Sung, T.E. Park, and Y.H. Yun, *Adv. Mater. Sci. Eng.*, 2015 (2015), 872730.
13. M. Balcerzak and M. Jurczyk, *Arch. Metall. Mater.*, 60 (2015) 1335.
14. Y.H. Hon, J.Y. Wang and Y.N. Pan, *Mater. Trans.*, 44 (2003) 2384.
15. H. Matsumoto, S. Watanabe and S. Hanada, *J. Alloy Compd.*, 439 (2007) 146.
16. Y. L. Zhou and M. Niinomi, *J. Alloys Compd.*, 466 (2008) 535.
17. A.P.R. Alves, F.A. Santana, L.A.A. Rosa, S.A. Cursino and E.N. Codaro, *Mater. Sci. Eng. C*, 24 (2004) 693.
18. N.T.C. Oliveira and A.C. Gaustaldi, *Acta Biomater.* 5 (2009) 399.
19. Y.L. Zhou and D.M. Luo, *J. alloy Compd.*, 509 (2011) 6267.
20. L.H. de Almeida, I.N. Bastos, I.D. Santos, A.J.B. Dutra, C.A. Nunes and S.B. Gabriel, *J. Alloy Compd.*, 615 (2014) S666-S669
21. J.L. Murry, Phase Diagram of Binary Titanium Alloys, ASM International, Metal Park, OH, 1987.
22. S.Y. Yu and J.R. Scully, *Corrosion*, 53 (1997) 965.
23. A. Choubey, B. Basu and R. Balasubramaniam, *Trends Biomater. Artif. Organs*, 18 (2005) 64.
24. I. Cvijović-Alagić, Z. Cvijović , S. Mitrović, V. Panić, M. Rakin, *Corrosion Sci.*, 53 (2011) 796.
25. W. S. Lee, C. F. Lin, T. H. Chen and H. W. Chen, *Mater. Sci. Eng. A*, 528 (2011) 6279.
26. A. S. Khan, Y. S. Suh and R. Kazmi, *Int. J. Plasticity*, 20 (2004) 2233
27. T.H. Chen and C.K. Tsai, Kai, *Materials***,** 8 (2015) 1831.
28. W. S. Lee, T.H. Chen, C.F. Lin and W. Z Lu, *Metall. Mater. Trans. A*, 43 (2012) 3998.
29. W. S. Lee, T.H. Chen, C.F. Lin and N. W. Lee, *Mater. Sci. Technol.*, 26 (2010) 720.
30. P. S. Follansbee and U. F. Kocks, *Acta Metall.*, 36 (1988) 81-93.
31. W. S. Lee and C. F. Lin, *Metall. Mater. Trans. A*, 33 (2002) 2801

32. C. Delgado-Alvarado and P.A. Sundaram, *Corrosion Sci.,* 49 (2007) 3732.
33. I.M. Pohrelyuk, V.M. Fedirko, O.V. Tkachuk and R.V. Proskurnyak, *Corrosion Sci.,* 66 (2013) 392.
34. H. Zohdi, H.R. Shahverdi and S.M.M. Hadavi, *Electrochem. Commun.,* 13 (2011) 840.
35. S. Sharma, A. N. Majila , V. M .Chavan, D.C. Fernando, R. J. Patel and S. N. Babu, *Procedia Eng.*, 173 (2017) 1894.
36. E. Chlebus, B. Kuźnicka, T. Kurzynowski, B. Dybała, *Mater. Charac.,* 62 (2011) 488.
37. W.S. Lee and C.H. Kao, *Mater. Sci. Eng. A,* 677 (2016) 230
38. S. Kobayashi, S. Nakagawa, K. Nakai and Y. Ohmori, *Mater. Trans.*, 43 (2002) 2956